SCIENCE CHINA
Information Sciences

• RESEARCH PAPER •

March 2023, Vol. 66 132304:1–132304:10
https://doi.org/10.1007/s11432-021-3497-6

Asynchronous multilevel bit-interleaved polar-coded modulation

Yaoyue HU[1], Zhiwen PAN[1,2*] & Yongliang GUAN[3]

[1]*National Mobile Communications Research Laboratory, Southeast University, Nanjing* 210096*, China;*
[2]*Purple Mountain Laboratories, Nanjing* 211100*, China;*
[3]*School of Electrical and Electronic Engineering, Nanyang Technological University, Singapore* 639798*, Singapore*

Received 19 September 2021/Revised 4 March 2022/Accepted 18 May 202/Published online 21 February 2023

Abstract Asynchronous bit-interleaved polar-coded modulation (A-BIPCM) provides high performance gain over conventional synchronous polar-coded modulation schemes at the expense of higher storage and decoding complexity. To overcome this drawback, this paper proposes a low-complexity polar-coded modulation, referred to as asynchronous multilevel bit-interleaved polar-coded modulation (A-MLBIPCM). The proposed A-MLBIPCM combines spatial coupling and the multilevel structure on polar-coded modulation. By analyzing the polarization diversity and storage complexity of the system, optimal encoding and modulation patterns are proposed to maintain the polarization diversity and reduce the storage complexity. Simulation results show that A-MLBIPCM provides better block-error-rate (BLER) performance than multilevel polar-coded modulation (MLPCM). Compared with A-BIPCM, the proposed scheme delivers about 23.84%–27.34% savings in storage and up to 33.02% savings in calculation complexity with almost no penalty in BLER (the difference is less than 0.1 dB).

Keywords polar codes, bit-interleaved coded modulation, multilevel coded modulation, spatial coupling, multi-stage decoding

Citation Hu Y Y, Pan Z W, Guan Y L. Asynchronous multilevel bit-interleaved polar-coded modulation. Sci China Inf Sci, 2023, 66(3): 132304, https://doi.org/10.1007/s11432-021-3497-6

1 Introduction

Polar codes are a family of error-correcting codes with explicit construction to achieve the capacity of binary input memoryless output symmetric channels with low encoding and decoding complexity [1]. To further improve spectral efficiency, polar codes are combined with high-order modulation, referred to as polar-coded modulation. Both multilevel polar-coded modulation (MLPCM) and bit-interleaved polar-coded modulation (BIPCM) have been investigated.

MLPCM [2] with set partition labeling and multistage decoding is an optimal polar-coded modulation from an information-theoretic point of view. In [3], a new framework for agile and robust construction of MLPCM is proposed for practical 5G systems. In [4], non-binary MLPCM and multi-kernel-based MLPCM are proposed for high mobility communications. In [5], polar lattice codes are proposed by using the multilevel construction to achieve the capacity of the additive white Gaussian noise (AWGN) channel. At the receiver, the multi-stage lasting successive-cancellation-list (L-SCL) based decoding approach [6] and the glued successive-cancellation list (G-SCL) decoding algorithm [7] have been proposed to improve the system performance by passing multiple decoded paths between two layers. Compared with the separate successive-cancellation list decoding approach where only one path is delivered between two layers, the above studies can achieve favorable performance gain with negligible increase of decoding complexity.

In contrast, BIPCM with Gray labeling results in large mutual information loss and thus a poor system performance [2,8]. There are some notable studies about bit-interleaved polar-coded modulation. To adapt arbitrary 2^q $(q = 1, 2, \ldots)$ modulation orders, punctured polar codes and multi-kernel [9] polar

* Corresponding author (email: pzw@seu.edu.cn)

codes are adopted in [8, 10], respectively. To improve the error-rate performance, partially information coupled BIPCM [11] is proposed by combining partially information coupled polar codes with direct BIPCM, punctured BIPCM, and multi-kernel BIPCM to achieve spatial coupling gain. In [12,13], shaped polar-coded modulation is investigated to achieve shaping gain. In [14], BIPCM with iterative decoding is investigated to trade off error-rate performance with complexity and latency.

All the above studies can be deemed as a synchronous modulation scheme where all the transmitted symbols in each frame come from one coded block. Recently, Ref. [15] proposed an asynchronous BIPCM, referred to as asynchronous bit-interleaved polar-coded modulation (A-BIPCM). In A-BIPCM, several different coded blocks are involved in the modulation of a transmitted frame in a spatial coupled way. Compared to MLPCM and BIPCM, A-BIPCM provides an improved block-error-rate (BLER) performance at the expense of higher storage complexity at both the transmitter and the receiver. For a 2^m-ary (suppose m is a power of two) A-BIPCM with frame length N, the transmitted symbols in each frame come from m coded blocks of size mN. These m coded blocks need to be stored at the transmitter for modulation. While at the receiver, a cache that can store $2^m mN$ symbol likelihoods and $(m-1)$ coded blocks is necessary for demodulation and decoding.

Apart from multilevel coded modulation and bit-interleaved coded modulation, a generalized coded modulation approach, multilevel bit-interleaved coded modulation, was proposed in [16] by embedding bit-interleaved coded modulation in a multilevel manner. Multilevel bit-interleaved coded modulation has been extensively studied in various communication and signal processing applications, such as non-orthogonal multiple access channels [17], broadcast channels [18–20], and multi-input multi-output systems [21]. Ref. [18] proposed a novel transmitter and receiver architecture for multilevel bit-interleaved low-density-parity-check coded modulation. When combined with polar codes, multilevel bit-interleaved coded modulation can mitigate information loss and require less encoder and decoder levels compared with BIPCM, thus resulting in improved BLER performance and reduced decoding complexity.

Motivated by the benefits of multilevel bit-interleaved polar-coded modulation, this paper proposes a low-complexity asynchronous polar-coded modulation, referred to as asynchronous multilevel bit-interleaved polar-coded modulation (A-MLBIPCM), aimed at reducing the storage and calculation complexity while maintaining good BLER performance. The main contributions of this paper are summarized as follows.

- The system model of A-MLBIPCM including the transmitter and a modified L-SCL-based receiver is introduced. Compared with A-BIPCM, the proposed A-MLBIPCM system enjoys the advantage of the multilevel structure, which leads to fewer coded blocks that are superposed in the spatial coupled structure and the shorter code length at each-level decoder. Thus, the storage and decoding complexity can be reduced.
- The polarization diversity of A-MLBIPCM is analyzed and compared with A-BIPCM and MLPCM.
- Optimal encoding and modulation patterns are proposed to maintain the polarization diversity as well as to reduce the storage complexity.

The rest of this paper is organized as follows. Section 2 presents the proposed A-MLBIPCM system. The polarization diversity of the system is analyzed in Section 3. Section 4 focuses on designing optimal encoding and modulation patterns. Simulations and comparisons are done in Section 5. Finally, the conclusion is made in Section 6.

Notations. Throughout the paper, channels are denoted by sans-serif fonts, such as B or W. $\mathbb{B}^{N\times M}$ represents $N\times M$ dimensional binary number field. The calligraphic characters, e.g., $\mathcal{S}, \mathcal{U}$, stand for sets. $\{\mathcal{U}\backslash\mathcal{S}\}$ represents a set whose elements belong to $\mathcal{U}$ but not to $\mathcal{S}$. Lowercase bold letters and capital bold symbols denote row vectors and matrices, respectively. For some row vector $\boldsymbol{a}$ of length N_a, $\boldsymbol{a}_{i:i'}$ stands for the entries with indices $i, i+1, \ldots, i'$, where $1 \leqslant i < i' \leqslant N_a$.

2 System model

2.1 Transmitter

The transmitter diagram of the proposed A-MLBIPCM is shown in Figure 1, where Π stands for the interleaver. For a 2^m-ary A-MLBIPCM with frame length N, at the t-th ($t = 1, 2, \ldots$) time instance, an mN-length source bit sequence $\boldsymbol{a}(t)$, including information bits $\boldsymbol{a}^{\mathcal{A}}(t)$ of length N_A and frozen bits $\boldsymbol{a}^{\bar{\mathcal{A}}}(t)$ of length $mN - N_A$, is decomposed into K-layer bit streams $\boldsymbol{a}^1(t), \boldsymbol{a}^2(t), \ldots, \boldsymbol{a}^K(t)$, where $\mathcal{A} \subseteq$

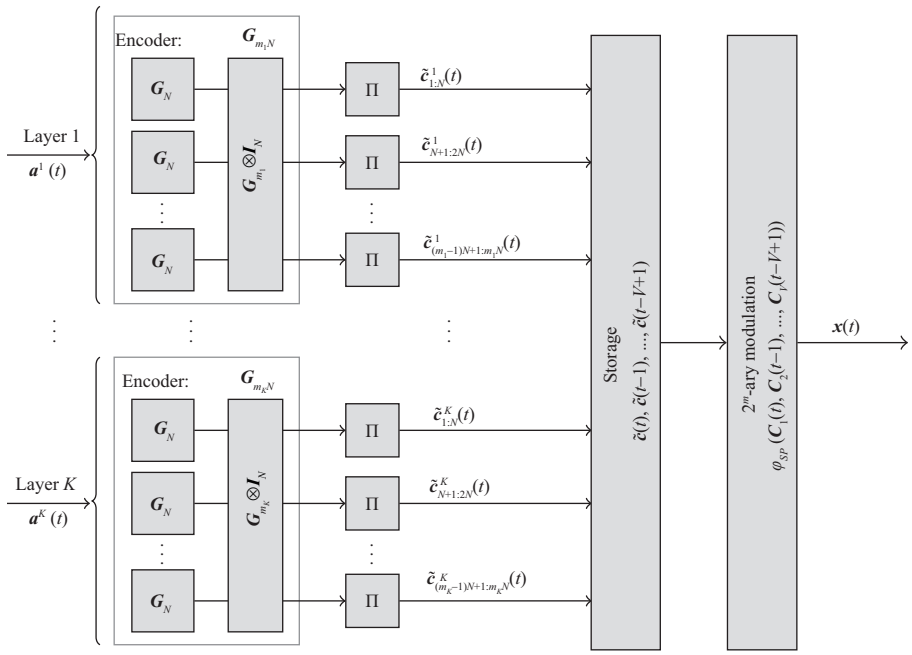

Figure 1 Transmitter diagram of the proposed A-MLBIPCM.

$\{1, 2, \ldots, mN\}$ is the information set and $\bar{\mathcal{A}}$ is the complementary set of $\mathcal{A}$. For each layer k ($k = 1, 2, \ldots, K$), $\boldsymbol{a}^k(t)$ is of length $m_k N$, where m_k is assumed to be a power of two and $\sum_{k=1}^{K} m_k = m$. Following the original polar encoding procedure, the coded bit sequence of layer k is

$$\begin{aligned} \boldsymbol{c}^k(t) &= \boldsymbol{a}^k(t)\boldsymbol{G}_{m_k N} = \boldsymbol{a}^k(t)\left(\boldsymbol{G}_N \otimes \boldsymbol{G}_{m_k}\right) \\ &= \boldsymbol{a}^k(t) \cdot \left(\boldsymbol{I}_{m_k} \otimes \boldsymbol{G}_N\right) \cdot \left(\boldsymbol{G}_{m_k} \otimes \boldsymbol{I}_N\right), \end{aligned} \tag{1}$$

where $\boldsymbol{G}_{m_k N} = \boldsymbol{F}_2^{\otimes \gamma_k}$ is the generator matrix of order $m_k N$. $\otimes$ denotes the Kronecker product. $\gamma_k = \log_2(m_k N)$. $\boldsymbol{F}_2 = \left(\begin{smallmatrix} 1 & 0 \\ 1 & 1 \end{smallmatrix}\right)$ is the Ariksn's original kernel. $\boldsymbol{G}_N = \boldsymbol{F}_2^{\otimes \beta}$, where $\beta = \log_2(N)$. $\boldsymbol{G}_{m_k} = \boldsymbol{F}_2^{\otimes(\gamma_k - \beta)}$. $\boldsymbol{I}_N$ and $\boldsymbol{I}_{m_k}$ are two identity matrices of order N and m_k, respectively.

$\boldsymbol{c}^k(t)$ is further decomposed to $m_k N$-length segments, i.e., $\boldsymbol{c}^k_{1:N}(t), \boldsymbol{c}^k_{N+1:2N}(t), \ldots, \boldsymbol{c}^k_{(m_k-1)N+1:m_k N}(t)$. The j-th ($j = 1, 2, \ldots, m_k$) segment $\boldsymbol{c}^k_{(j-1)N+1:jN}(t)$ is further interleaved to $\tilde{\boldsymbol{c}}^k_{(j-1)N+1:jN}(t)$. Combining all interleaved bit sequences, the interleaved coded block $\tilde{\boldsymbol{c}}(t)$ is

$$\tilde{\boldsymbol{c}}(t) = \left(\tilde{\boldsymbol{c}}^1(t), \tilde{\boldsymbol{c}}^2(t), \ldots, \tilde{\boldsymbol{c}}^K(t)\right) \tag{2}$$

with a total of mN-length segments.

Definition 1 (Encoding pattern)**.** The encoding pattern for a 2^m-ary K-layer A-MLBIPCM is defined as a set $\{\mathcal{S}_1, \mathcal{S}_2, \ldots, \mathcal{S}_K\}$, where subset $\mathcal{S}_k = \{s_{k,j} | j = 1, 2, \ldots, m_k\} \subseteq \{1, 2, \ldots, m\}$ and $s_{k,j}$ represents the bit index for which segment $\tilde{\boldsymbol{c}}^k_{(j-1)N+1:jN}(t)$ is served during the modulation process. Also, $\min(\mathcal{S}_1) < \min(\mathcal{S}_2) < \cdots < \min(\mathcal{S}_K)$, and $\mathcal{S}_1 \cup \mathcal{S}_2 \cup \cdots \cup \mathcal{S}_K = \{1, 2, \ldots, m\}$. For $1 \leqslant k' \neq k \leqslant K$, $\mathcal{S}_k \cap \mathcal{S}_{k'} = \emptyset$.

Definition 2 (Modulation pattern)**.** Suppose each transmitted frame $\boldsymbol{x}(t)$ comes from V successive coded blocks. The modulation pattern for a 2^m-ary V-spatially-coupled A-MLBIPCM is defined as a set $\{\mathcal{R}_1, \mathcal{R}_2, \ldots, \mathcal{R}_V\}$, where $1 \leqslant V \leqslant m$ and $\mathcal{R}_v$ ($v = 1, 2, \ldots, V$) is a set of size η_v, defined as

$$\mathcal{R}_v = \{m - \mu_v + \eta_v, m - \mu_v + \eta_v - 1, \ldots, m - \mu_v + 1\}, \tag{3}$$

where $\mu_v = \sum_{l=1}^{v} \eta_l$ and $\mu_V = \sum_{v=1}^{V} \eta_v = m$. For each block $\tilde{\boldsymbol{c}}(t)$, the segments with bit indices in $\mathcal{R}_v$ will be involved in the modulation of $\boldsymbol{x}(t + v - 1)$. Note that $\mathcal{R}_1 \cup \mathcal{R}_2 \cup \cdots \cup \mathcal{R}_V = \{m, m-1, \ldots, 1\}$. For $\forall\ v' = 1, 2, \ldots, V$ and $v' \neq v$, $\mathcal{R}_v \cap \mathcal{R}_{v'} = \emptyset$.

The modulation pattern relies on the encoding pattern. Given $\{\mathcal{S}_1, \mathcal{S}_2, \ldots, \mathcal{S}_K\}$, $\{\mathcal{R}_1, \mathcal{R}_2, \ldots, \mathcal{R}_V\}$ should satisfy the following two rules:

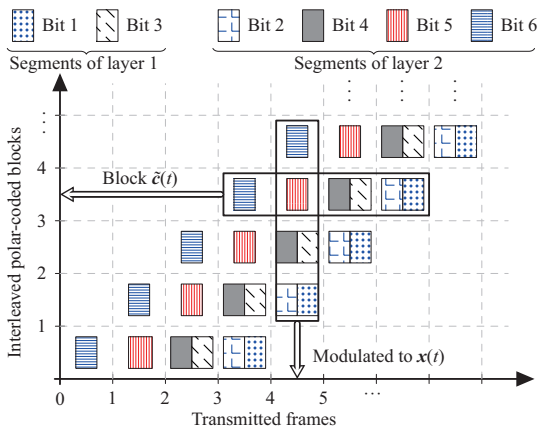

Figure 2 (Color online) An example of the modulation procedure of A-MLBIPCM.

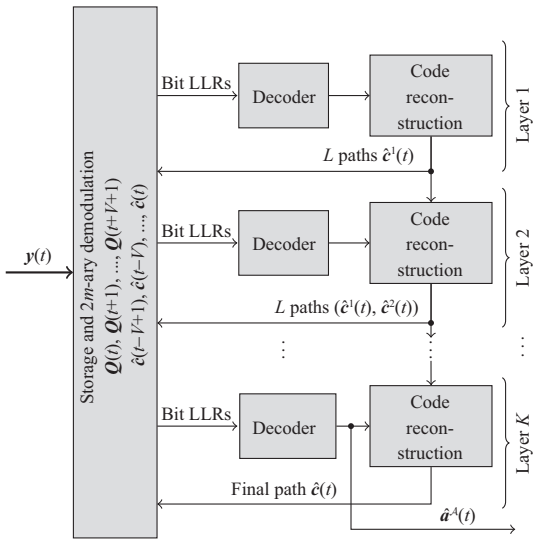

Figure 3 Receiver diagram of the proposed A-MLBIPCM.

(1) From [15], to reduce the interference among the segments at the same layer and enhance the polarization diversity, the segments of $\tilde{\boldsymbol{c}}_k(t)$ should be assigned to different transmitted frames. Hence, for $s_{k,j}, s_{k,j'} \in \mathcal{S}_k$ $(\forall\ j' \neq j)$, if $s_{k,j} \in \mathcal{R}_v$, then $s_{k,j'} \notin \mathcal{R}_v$.

(2) $\mathcal{S}_1 \subseteq \mathcal{U}$, where set $\mathcal{U}$ contains the smallest element of each $\mathcal{R}_v$, i.e.,

$$\mathcal{U} = \{m - \mu_1 + 1, m - \mu_2 + 1, \ldots, 1\}. \tag{4}$$

The generation of the optimal encoding and modulation patterns will be introduced in Section 4.

Given $\{\mathcal{S}_1, \mathcal{S}_2, \ldots, \mathcal{S}_K\}$ and $\{\mathcal{R}_1, \mathcal{R}_2, \ldots, \mathcal{R}_V\}$, each block $\tilde{\boldsymbol{c}}(t)$ will be served for V successive transmitted frames $\boldsymbol{x}(t), \boldsymbol{x}(t+1), \ldots, \boldsymbol{x}(t+V-1)$. The transmitted symbol frame $\boldsymbol{x}(t)$ can be expressed as

$$\boldsymbol{x}(t) = \phi_{\mathrm{SP}}\left(\boldsymbol{C}_1(t), \boldsymbol{C}_2(t-1), \ldots, \boldsymbol{C}_V(t-V+1)\right), \tag{5}$$

where $\boldsymbol{C}_V(t-v+1)$ is a $\eta_v \times N$ matrix whose row vectors are the segments with bit indices in $\mathcal{R}_v$ of $\tilde{\boldsymbol{c}}(t-v+1)$. $\phi_{\mathrm{SP}} : \mathbb{B}^{m \times N} \to \mathcal{X}^N$ is the set partition labeling. $\mathcal{X}$ is the input alphabet of size 2^m. From (4), V successive coded blocks $\tilde{\boldsymbol{c}}(t), \tilde{\boldsymbol{c}}(t-1), \ldots, \tilde{\boldsymbol{c}}(t-V+1)$ are involved in the modulation of $\boldsymbol{x}(t)$. For $t \leqslant 0$, $\tilde{\boldsymbol{c}}(t)$ is set as an all-zero vector.

Figure 2 shows an example of the modulation procedure when $m = 6$. Here, $K = 2$, $V = 4$, $\{\mathcal{S}_1, \mathcal{S}_2\} = \{\{1,3\}, \{2,4,5,6\}\}$, and $\{\mathcal{R}_1, \mathcal{R}_2, \mathcal{R}_3, \mathcal{R}_4\} = \{\{6\}, \{5\}, \{4,3\}, \{2,1\}\}$.

2.2 Modified L-SCL decoder

The original L-SCL decoding algorithm [6] is a multi-stage structure that successively performs the demapping and decoding procedures layer by layer. At the end of each layer, L reconstructed paths and their path metrics will be sent to the next layer until the last layer selects the final path, as shown in Figure 3. Based on the system of A-MLBIPCM, the focus of the receiver design is to be adaptive to various encoding patterns. However, the original L-SCL decoding scheme is proposed for joint demodulation and decoding in synchronous MLPCM, which is a special case of A-MLBIPCM with a specific encoding pattern. Hence, the original L-SCL is not applicable for the proposed A-MLBIPCM. To solve this problem, we modified the demodulation process of L-SCL according to the encoding and modulation patterns. Compared with the original L-SCL, the modified L-SCL decoding has a similar decoding process as original L-SCL, but is adaptive to A-MLBIPCM with arbitrary encoding patterns.

Assume $\hat{\boldsymbol{a}}^{\mathcal{A}}(t)$, $\hat{\boldsymbol{c}}(t)$, and $\hat{\boldsymbol{c}}^k(t)$ are the estimates of $\boldsymbol{a}^{\mathcal{A}}(t)$, $\tilde{\boldsymbol{c}}(t)$, and $\tilde{\boldsymbol{c}}^k(t)$. To formulate L-SCL, without loss of generality, the symbol likelihoods of the received frame $\boldsymbol{y}(t)$ under the AWGN channel with noise variance σ^2 are computed as

$$[\boldsymbol{Q}(t)]_{p,q} \propto \exp\left(-\frac{|[\boldsymbol{y}(t)]_q - x_p|^2}{2\sigma^2}\right), \tag{6}$$

where $p = 1, 2, \ldots, 2^m$ and $q = 1, 2, \ldots, N$. x_p is the p-th entry of $\mathcal{X}$. $[\boldsymbol{Q}(t)]_{p,q}$ is the (p, q)-th entry of matrix $\boldsymbol{Q}(t)$. To retrieve $\tilde{\boldsymbol{c}}(t)$ or $\hat{\boldsymbol{a}}^{\mathcal{A}}(t)$, one cache that can store $\boldsymbol{Q}(t), \boldsymbol{Q}(t+1), \ldots, \boldsymbol{Q}(t+V-1)$ and $\hat{\boldsymbol{c}}(t-1), \hat{\boldsymbol{c}}(t-2), \ldots, \hat{\boldsymbol{c}}(t-V+1)$ is required at the receiver.

For $\forall\, u \in \mathcal{U}$, with the knowledge of the segments with bit indices $\{1, 2, \ldots, u-1\}$ stored in previously reconstructed blocks $\hat{\boldsymbol{c}}(t-1), \hat{\boldsymbol{c}}(t-2), \ldots, \hat{\boldsymbol{c}}(t-V+1)$, the demodulation for the segment with bit index u can be executed by using the symbol likelihoods stored in $\boldsymbol{Q}(t), \boldsymbol{Q}(t+1), \ldots, \boldsymbol{Q}(t+V-1)$. Initialize L path metrics as 0. Since $\mathcal{S}_1 \subseteq \mathcal{U}$, the first layer can complete successive-cancellation list decoding and code reconstruction, thus outputting L paths of $\hat{\boldsymbol{c}}^1(t)$ along with their path metrics to the next layer. Then, as conventional L-SCL decoding, the decoder at layer k ($k = 2, \ldots, K$) is initialized with L paths whose metrics are set to the path metrics output by layer $(k-1)$. With the knowledge of L paths of $(\hat{\boldsymbol{c}}^1(t), \ldots, \hat{\boldsymbol{c}}^{k-1}(t))$ and demodulation messages of the segments with bit indices in $\{\mathcal{U} \backslash \mathcal{S}_1\}$, demodulation, decoding, and code reconstruction can be successively done. At the end of layer k (except $k = K$), L paths of $(\hat{\boldsymbol{c}}^1(t), \ldots, \hat{\boldsymbol{c}}^k(t))$ along with their path metrics are output and sent to layer $(k+1)$. As for layer K, the final path $\hat{\boldsymbol{c}}(t)$ or $\hat{\boldsymbol{a}}^{\mathcal{A}}(t)$ with the maximum metric or that can pass the cyclic redundancy check (CRC) will be selected as the output. Note that $\hat{\boldsymbol{c}}(t)$ will be further stored at the receiver cache for the decoding of next block.

Take the modulation case of Figure 2 as an example. Here, $\mathcal{U} = \{6, 5, 3, 1\}$. With the knowledge of the segments stored in previously reconstructed blocks $\hat{\boldsymbol{c}}(t-1), \hat{\boldsymbol{c}}(t-2), \ldots, \hat{\boldsymbol{c}}(t-3)$, the bit log-likelihood ratios for the segments of $\boldsymbol{c}(t)$ with bit indices in $\mathcal{U}$ can be obtained. Then, the first layer conducts successive-cancellation list decoding and code reconstruction, thus outputting L paths of $\hat{\boldsymbol{c}}^1(t)$ along with their path metrics to the next layer. Further, through demodulation, the bit log-likelihood ratios for the segments of $\boldsymbol{c}(t)$ with bit indices in $2, 4$ can be obtained. Finally, the second layer can complete decoding.

3 Polarization diversity analysis

In this section, the polarization diversity of A-MLBIPCM is analyzed and compared with that of A-BIPCM and MLPCM. The mean and variance of the bit-polarized-channel capacities are used to analyze the polarization diversity as in [2,15].

The bit polarized channels of A-MLBIPCM are generated through two channel transforms during the modulation and encoding processes. The channel transform of the modulation process maps a discrete memoryless channel (DMC) $\mathsf{W} : \mathcal{X} \to \mathcal{Y}$ with input alphabet $\mathcal{X}$ and an arbitrary output alphabet $\mathcal{Y}$ to K sets of binary-input DMCs, defined as

$$\mathsf{W} \to \{\mathsf{B}_{1,1}, \ldots, \mathsf{B}_{1,m_1}\}, \ldots, \{\mathsf{B}_{K,1}, \ldots, \mathsf{B}_{K,m_K}\}, \tag{7}$$

where $\mathsf{B}_{k,j}$ is given by

$$\mathsf{B}_{k,j} : \{0,1\} \to \mathcal{Y} \times \{0,1\}^{s_{k,j}-1}. \tag{8}$$

Note that due to the chain rule of mutual information, the mutual information of W satisfies $I(\mathsf{W}) = \sum_{k=1}^{K} \sum_{j=1}^{m_k} I(\mathsf{B}_{k,j})$, which is independent of the encoding pattern.

The channel transform $\boldsymbol{G}_{m_k N}$ of the encoding process can be seen as a two-step procedure [15]. The first step transforms $\{\mathsf{B}_{k,1}, \mathsf{B}_{k,2}, \ldots, \mathsf{B}_{k,m_k}\}$ to $\{\bar{\mathsf{B}}_{k,1}, \bar{\mathsf{B}}_{k,2}, \ldots, \bar{\mathsf{B}}_{k,m_k}\}$ by using the parallel channel transform $\boldsymbol{G}_{m_k}$. Then, $\boldsymbol{G}_N$ is applied to N groups of $\bar{\mathsf{B}}_{k,j}$ to generate $m_k N$ bit polarized channels $\{\mathsf{B}_{m_k N}^{(1)}, \mathsf{B}_{m_k N}^{(2)}, \ldots, \mathsf{B}_{m_k N}^{(m_k N)}\}$. When $K = 1$, the channel transform is equivalent to A-BIPCM; when $K = m$, the first step can be neglected since $\boldsymbol{G}_{m_k} = 1$, and the channel transform is equivalent to MLPCM. In this regard, A-MLBIPCM is a generalization of A-BIPCM and MLPCM.

Proposition 1. The polarization diversity of A-MLBIPCM is superior to that of MLPCM but inferior to that of A-BIPCM when m is a power of two.

Proof. When m is a power of two, after the first step, $\{\bar{\mathsf{B}}_{k,1}, \bar{\mathsf{B}}_{k,2}, \ldots, \bar{\mathsf{B}}_{k,m_k}\}$ satisfies [15]

$$\sum_{k=1}^{K} \sum_{j=1}^{m_k} (I(\bar{\mathsf{B}}_{k,j})) = \sum_{i=1}^{m} (I(\mathsf{B}_i)) = \sum_{i=1}^{m} (I(\hat{\mathsf{B}}_i)) = m I(\mathsf{W}), \tag{9}$$

$$\sum_{i=1}^{m} (I(\mathsf{B}_i))^2 \leqslant \sum_{k=1}^{K} \sum_{j=1}^{m_k} (I(\bar{\mathsf{B}}_{k,j}))^2 \leqslant \sum_{i=1}^{m} (I(\hat{\mathsf{B}}_i))^2, \tag{10}$$

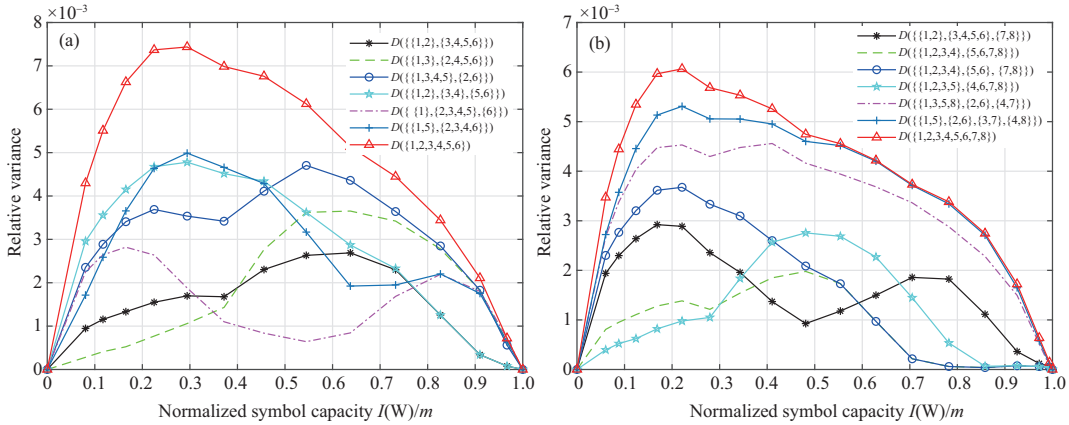

Figure 4 (Color online) The relative variances of A-BIPCM [15] with respect to the proposed A-MLBIPCM with different $\{\mathcal{S}_1, \mathcal{S}_2, \ldots, \mathcal{S}_K\}$ and MLPCM [6]. (a) 64-QAM; (b) 256-QAM.

where B_i is a binary-input DMC, defined as $\mathsf{B}_i : \{0,1\} \to \mathcal{Y} \times \{0,1\}^{i-1}$. $\hat{\mathsf{B}}_1, \hat{\mathsf{B}}_2, \ldots, \hat{\mathsf{B}}_m$ are the transformed channels by applying $\boldsymbol{G}_m$ to $\mathsf{B}_1, \mathsf{B}_2, \ldots, \mathsf{B}_m$, i.e., the first-step channel transform of A-BIPCM.

According to [15], the sum capacity of all the bit polarized channels at layer k equals $N \sum_{j=1}^{m_k} I(\mathsf{B}_{k,j})$. Thus, the mean capacity of all the bit polarized channels of A-MLBIPCM is $\frac{1}{m} I(\mathsf{W})$, which is the same as that of MLPCM and A-BIPCM. The variance capacity is

$$\mathrm{var}_{\text{A-MLBI}} = \frac{1}{mN} \sum_{k=1}^{K} \sum_{w=1}^{m_k N} I(\mathsf{B}_{m_k N}^{(w)})^2 - \frac{1}{m^2} I(\mathsf{W})^2, \tag{11}$$

and satisfies [15]

$$\mathrm{var}_{\text{ML}} \leqslant \mathrm{var}_{\text{A-MLBI}} \leqslant \mathrm{var}_{\text{A-BI}}, \tag{12}$$

where var_{ML} and $\mathrm{var}_{\text{A-BI}}$ denote the variances of bit-polarized-channel capacities of MLPCM and A-BIPCM, respectively. Eq. (12) proves Proposition 1.

Define the relative variance of A-BIPCM with respect to A-MLBIPCM as

$$D(\{\mathcal{S}_1, \mathcal{S}_2, \ldots, \mathcal{S}_K\}) = \mathrm{var}_{\text{A-BI}} - \mathrm{var}_{\text{A-MLBI}}. \tag{13}$$

Figure 4 shows the relative variances of A-BIPCM with respect to A-MLBIPCM with different $\{\mathcal{S}_1, \ldots, \mathcal{S}_K\}$ under the normalized symbol capacity. Also, the relative variance of A-BIPCM with respect to MLPCM, i.e., $D(\{1, 2, \ldots, m\}) = \mathrm{var}_{\text{A-BI}} - \mathrm{var}_{\text{ML}}$, is plotted as a comparison. 2^m-ary quadrature amplitude modulations (2^m-QAM) at $m = 6,\ 8$ are adopted. N is set as 128. The specific values of $\{\mathcal{S}_1, \mathcal{S}_2, \ldots, \mathcal{S}_K\}$ are given in the legends. For 64-QAM, the puncturing technique is applied to A-BIPCM to obtain $6N$ coded bits. We observe that the polarization diversity of A-MLBIPCM depends on both the normalized symbol capacity and encoding patterns. MLPCM has the worst polarization diversity. Compared with A-BIPCM, A-MLBIPCM has similar or slightly worse polarization diversity at some normalized symbol capacity. This indicates that A-MLBIPCM may have similar BLER performance as A-BIPCM. Also, Figure 4 shows that different encoding patterns may have similar polarization diversity and thus similar BLER performance. For example, when the normalized symbol capacity is larger than 0.72, the two encoding patterns $\{\{1, 2\}, \{3, 4, 5, 6\}\}$ and $\{\{1, 2\}, \{3, 4\}, \{5, 6\}\}$ have the same polarization diversity.

4 Optimal encoding and modulation pattern design

From Section 3, to design the A-MLBIPCM, on one hand, the encoding patterns should have similar polarization diversity as A-BIPCM to maintain the BLER performance, and there might exist multiple encoding patterns that can satisfy this rule. On the other hand, as we will show in Section 5, V should be minimized to reduce the storage complexity. Therefore, the encoding and modulation patterns that generate similar polarization diversity and the smallest V should be chosen as the final results. Based on

these two rules, an effective method to generate optimal encoding and modulation patterns is proposed in this section. The generation procedure is detailed as follows.

Step 1. Generate all possible encoding patterns $\{\mathcal{S}_1, \mathcal{S}_2, \ldots, \mathcal{S}_K\}$ that satisfy $\sum_{k=1}^{K} m_k = m$, where m_k is a power of two.

Step 2. For each set $\{\mathcal{S}_1, \mathcal{S}_2, \ldots, \mathcal{S}_K\}$, compute $D(\{\mathcal{S}_1, \mathcal{S}_2, \ldots, \mathcal{S}_K\})$, and choose the sets that satisfy $D(\mathcal{S}_1, \mathcal{S}_2, \ldots, \mathcal{S}_K) \leqslant \epsilon$, denoted by $\{\bar{\mathcal{S}}_1, \bar{\mathcal{S}}_2, \ldots, \bar{\mathcal{S}}_{\bar{K}}\}$. The parameter ϵ depends on specific values of code rate R, m, and N, and can be obtained through off-line simulation.

Step 3. For each set $\{\bar{\mathcal{S}}_1, \bar{\mathcal{S}}_2, \ldots, \bar{\mathcal{S}}_{\bar{K}}\}$, execute Algorithm 1 to get corresponding set $\bar{\mathcal{U}}$ with $\bar{V}$ elements.

Algorithm 1 Generation of $\mathcal{U}$

Require: $\mathcal{S}_1, \mathcal{S}_2, \ldots, \mathcal{S}_K$;
Ensure: Set $\mathcal{U}$ with V elements;
Initialize Elements in each $\mathcal{S}_k$ are arranged in ascending order; $\mathcal{U} = \emptyset$, and $V = 0$;
for $k = K$; $k \geqslant 1$; $k--$ **do**
  for $j = m_k$; $j \geqslant 1$; $j--$ **do**
    $v \leftarrow 1$;
    while $v \leqslant V$ **do**
      if $\mathcal{S}_k[j] = \mathcal{U}[v] - 1$ **and** $\mathcal{U}[v] \notin \mathcal{S}_k$ **then**
        $\mathcal{U}[v] \leftarrow \mathcal{S}_k[j]$;
        break;
      else
        $v \leftarrow v + 1$;
      end if
    end while
    if $v = V + 1$ **then**
      $\mathcal{U}[++V] \leftarrow \mathcal{S}_k[j]$;
    end if
  end for
end for

Step 4. Let $V^{\dagger} = \min(\bar{V})$. Compute

$$\{\mathcal{S}_1^{\dagger}, \mathcal{S}_2^{\dagger}, \ldots, \mathcal{S}_{K^{\dagger}}^{\dagger}\} = \arg \min_{\{\bar{\mathcal{S}}_1, \ldots, \bar{\mathcal{S}}_K\}} (\bar{V}). \tag{14}$$

$\{\mathcal{S}_1^{\dagger}, \mathcal{S}_2^{\dagger}, \ldots, \mathcal{S}_{K^{\dagger}}^{\dagger}\}$ is the final encoding pattern.

Step 5. Based on (3) and (4), the final modulation pattern is $\{\mathcal{R}_1^{\dagger}, \mathcal{R}_2^{\dagger}, \ldots, \mathcal{R}_{V^{\dagger}}^{\dagger}\}$, where $\mathcal{U}^{\dagger}$ is the output of Algorithm 1 with input $\{\mathcal{S}_1^{\dagger}, \mathcal{S}_2^{\dagger}, \ldots, \mathcal{S}_{K^{\dagger}}^{\dagger}\}$. $\mathcal{R}_1^{\dagger} = \{m, m-1, \ldots, \mathcal{U}^{\dagger}[1]\}$. For $v' = 2, 3, \ldots, V^{\dagger}$, $\mathcal{R}_{v'}^{\dagger} = \{\mathcal{U}^{\dagger}[v'-1] - 1, \mathcal{U}^{\dagger}[v'-1] - 2, \ldots, \mathcal{U}^{\dagger}[v']\}$.

5 Simulation results

This section provides some numerical results in terms of the BLER performance and the calculation and storage complexity. The number of CRC bits and list size L is set to 8. Both 64-QAM and 256-QAM are considered. The frame length N is set to 128.

5.1 BLER performance

Figure 5 shows the BLER performance of A-MLBIPCM, A-BIPCM, and MLPCM under AWGN channels at 64-QAM. For A-MLBIPCM, the optimized encoding patterns at $R = 1/4$ and $R = 1/2$ are $\{\{1, 3\}, \{2, 4, 5, 6\}\}$ and $\{\{1\}, \{2, 3, 4, 5\}, \{6\}\}$, respectively. The BLER performance of A-MLBIPCM with a random encoding pattern $\{\{1, 2\}, \{3, 4\}, \{5, 6\}\}$ is also shown in Figure 5. As seen from Figure 5, the BLER performance of A-MLBIPCM with the optimized encoding pattern is close to that of A-BIPCM and is better than that of A-MLBIPCM with the random pattern $\{\{1, 2\}, \{3, 4\}, \{5, 6\}\}$.

A further BLER comparison of the proposed optimized A-MLBIPCM, A-BIPCM, and MLPCM at 256-QAM is illustrated in Figure 6. The optimized encoding patterns of A-MLBIPCM at $R = 1/4$ and $R = 1/2$ are $\{\{1, 2, 3, 5\}, \{4, 6, 7, 8\}\}$ and $\{\{1, 2\}, \{3, 4, 5, 6\}, \{7, 8\}\}$, respectively. As in Figure 5, Figure 6 shows that the proposed optimized A-MLBIPCM behaves similarly as A-BIPCM with less than 0.1 dB performance gap. Note that both Figures 5 and 6 are inconstant with the polarization

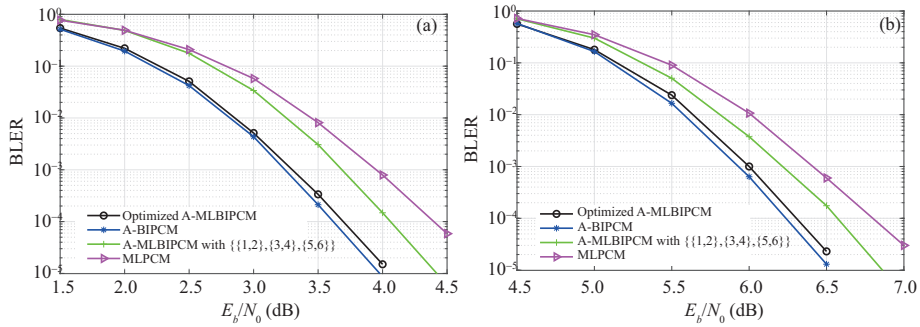

Figure 5 (Color online) BLER performance of the proposed A-MLBIPCM, A-BIPCM [15], and MLPCM [6] at 64-QAM. (a) $R = 1/4$; (b) $R = 1/2$.

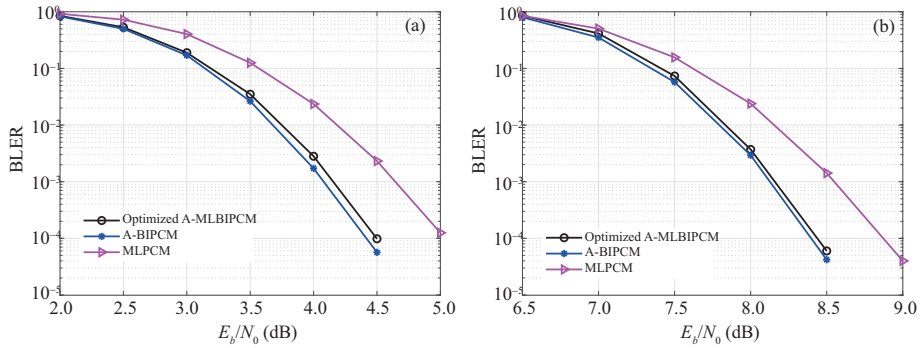

Figure 6 (Color online) BLER performance of the proposed A-MLBIPCM, A-BIPCM [15], and MLPCM [6] at 256-QAM. (a) $R = 1/4$; (b) $R = 1/2$.

diversity results as shown in Figure 4. This demonstrates the effectiveness of the optimization on encoding patterns. In addition, compared with MLPCM, the proposed optimized A-MLBIPCM achieves 0.45–0.7 dB performance gain at BLER = 10^{-4} due to its better polarization diversity.

5.2 Complexity analysis

This subsection considers the receiver complexity of the proposed A-MLBIPCM in terms of de-mapping, decoding, and storage, especially compared with the other two modulation schemes.

5.2.1 *Calculation complexity*

In this subsection, flop count is used as the metric to evaluate the calculation complexity of de-mapping and decoding one message. As in [22], each complex addition requires two flops and each complex multiplication requires six flops. Logarithmic and exponential operations, which are typically calculated using rational polynomial interpolation, require 20 flop.

For de-mapping complexity analysis, the proposed A-MLBIPCM follows bit-level-based multi-stage de-mapping as A-BIPCM and MLPCM. The bit logarithm likelihood ratios (LLRs) can be calculated as

$$\lambda_{i,q} = \ln \frac{\sum_{x_p \in \mathcal{X}_i^+} [\boldsymbol{Q}(t)]_{p,q}}{\sum_{x_p \in \mathcal{X}_i^-} [\boldsymbol{Q}(t)]_{p,q}}. \tag{15}$$

Eq. (15) has one log operation and one divide operation per received symbol $[\boldsymbol{y}(t)]_q$. From (6), the calculation of $[\boldsymbol{Q}(t)]_{p,q}$ requires 31 flop. Hence, the calculation of $\boldsymbol{Q}(t)$ requires $31 \times 2^m N$ flop. When $i = 1$, the sets $\mathcal{X}_i^+$ and $\mathcal{X}_i^-$ have 2^{m-1} elements. The summation operator adds these elements $[\boldsymbol{Q}(t)]_{p,q}$ in the numerator and denominator requiring $(2^m - 2)$ additions. For $i = 2, 3, \ldots, m$, $\mathcal{X}_i^+$ or $\mathcal{X}_i^-$, which depends on the knowledge of the decoded bits of previous level $i' = 1, 2, \ldots, i-1$, is half the size of $\mathcal{X}_{i-1}^+$. Eq. (15) requires $(2^{m-i+1} - 2)$ additions.

For MLPCM, L reconstructed paths of previous levels will be sent to the next bit level. Hence, the decoded bits of previous levels of each received symbol have $\bar{L}_i = \min(2^{i-1}, L)$ results, resulting in

Table 1 Calculation complexity of the optimized A-MLBIPCM, A-BIPCM, and MLPCM at 64-QAM

Item	Number of flop			
	Optimized A-MLBIPCM ($R = 1/4$)	Optimized A-MLBIPCM ($R = 1/2$)	A-BIPCM	MLPCM
De-Mapping	315392	310016	284672	376448
Decoding	1730560	1664000	2662400	1397760
Total	2045952	1974016	2947072	1774208

Table 2 Calculation complexity of the optimized A-MLBIPCM, A-BIPCM, and MLPCM at 256-QAM

Item	Number of flop			
	Optimized A-MLBIPCM ($R = 1/4$)	Optimized A-MLBIPCM ($R = 1/2$)	A-BIPCM	MLPCM
De-Mapping	1170432	1153024	1100544	1291904
Decoding	2396160	2263040	2662400	1863680
Total	3682304	3416064	3762944	3761792

$(2^{m-i+1}-2)\bar{L}_i$ additions, $\bar{L}_i$ log operation, and $\bar{L}_i$ divide operation at each bit level. Therefore, the total number of flop per frame in MLPCM is $31 \times 2^m N + N\sum_{i=1}^{m} \bar{L}_i(2^{m-i+1}+19)$.

For A-BIPCM, there is only one reconstructed path delivered from previous levels. Therefore, the total number of flop per frame in A-BIPCM is $31 \times 2^m N + N\sum_{i=1}^{m}(2^{m-i+1}+19) = N(33 \times 2^m + 19m - 2)$.

For the proposed A-MLBIPCM, bit level $i \in \mathcal{U}$ will receive only one reconstructed path from previous levels; while bit level $i \in \{\{1,2,\ldots,m\}\backslash\mathcal{U}\}$ will receive L reconstructed path from previous levels. Therefore, the total number of flop per frame in A-MLBIPCM is $31 \times 2^m N + N\sum_{i\in\mathcal{U}}(2^{m-i+1}+19) + N\sum_{i\in\{\{1,2,\ldots,m\}\backslash\mathcal{U}\}} \bar{L}_i(2^{m-i+1}+19)$.

Next, consider the decoding complexity. At the receiver side, one successive cancellation decoder uses one decoder unit with two node calculations to decode received signals. According to [22], each decoder unit requires 65 flop and there are $\frac{m_k N}{2}\gamma_k$ decoder units at layer k. Since there are L successive cancellation decoders and K layers in the proposed A-MLBIPCM, the total number of flop is $\sum_{k=1}^{K} 32.5Lm_kN\gamma_k$. For MLPCM and A-BIPCM, the flop count is $32.5LmN\beta$ and $32.5L\bar{m}N\left(\lceil\log_2(m)\rceil+\beta\right)$, respectively, where $\bar{m} = 2^{\lceil\log_2(m)\rceil}$.

Tables 1 and 2 compare the calculation complexity of the optimized A-MLBIPCM, A-BIPCM, and MLPCM at 64-QAM and 256-QAM, respectively. It can be observed that A-MLBIPCM exhibits higher decoding complexity than MLPCM but lower decoding complexity than A-BIPCM, especially when m is not a power of two. The decoding complexity reduction of A-MLBIPCM compared with A-BIPCM is about 10%–37.5%. For 256-QAM, the calculation complexity of A-MLBIPCM is slightly lower than that of A-BIPCM and that of MLPCM. The calculation complexity reduction of A-MLBIPCM compared with A-BIPCM at 64-QAM reaches 5.22%–9.22%. For 64-QAM, the decoding complexity takes the dominant role in calculation complexity. The calculation complexity reduction of A-MLBIPCM compared with A-BIPCM at 64-QAM reaches 30.85%–33.02%.

5.2.2 *Storage complexity*

Finally, the storage complexity comes from storing symbol likelihoods, bit LLRs, intermediate bits, and path metrics. For simplicity, in the following, the number of quantized bits to represent symbol likelihoods, bit LLRs, and path metrics is the same and fixed as N_{LLR}. The number of bits required in storage is used as the metric for storage complexity evaluation.

For A-MLBIPCM, except for L paths of N_A-length information bits and L path metrics, the SCL decoder needs to store $(m'N-1)\,L$ intermediate bit LLRs and $2\,(m'N-1)\,L$ intermediate bits, where $m' = \max_{1\leqslant k\leqslant K}(m_k)$. At the de-mapper, a total of $2^m VN$ symbol likelihoods include $\boldsymbol{Q}(t), \boldsymbol{Q}(t+1), \ldots, \boldsymbol{Q}(t+V-1)$ and need to be stored. Also, the de-mapper requires to store $m'NL$ bit LLRs and $((Vm - \sum_{v=1}^{V}\mu_v)N + (m-m_K)NL)$ reconstructed coded bits. Therefore, the total storage is $(2^m V + 2m'L)NN_{\mathrm{LLR}} + (mN + 2m'N + N_A - m_K N - 2)L + (Vm - \sum_{v=1}^{V}\mu_v)N$.

For MLPCM, the SCL decoder is applied at m bit levels, which needs to store $(N-1)L$ intermediate bit LLRs, $2(N-1)L$ intermediate bits, L paths of N_A-length information bits, and L path metrics. The de-mapper requires $2^m N$ symbol likelihoods, NL bit LLRs, and $(m-1)NL$ reconstructed coded bits. Therefore, the total storage is $(2^m + 2L)NN_{\mathrm{LLR}} + (mN + N + N_A - 2)L$.

For A-BIPCM, the SCL decoder needs to store $(\bar{m}N-1)\,L$ intermediate bit LLRs, $2(\bar{m}N-1)L$

Table 3 Storage complexity of the optimized A-MLBIPCM, A-BIPCM, and MLPCM at 64-QAM and 256-QAM

Item	Number of bits (64-QAM)			Number of bits (256-QAM)		
	Optimized A-MLBIPCM	A-BIPCM	MLPCM	Optimized A-MLBIPCM	A-BIPCM	MLPCM
Symbol likelihoods	262144	393216	65536	1572864	2097152	262144
Total ($R = 1/4$)	341886	470512	93680	1655280	2176624	289776
Total ($R = 1/2$)	345200	472048	95216	1659376	2178672	291824

intermediate bits, L paths of N_A-length information bits, and L path metrics. The de-mapper requires $2^m mN$ symbol likelihoods, $\bar{m}N$ bit LLRs, and $m(m-1)N/2$ reconstructed coded bits. Therefore, the total storage is $(2^m m + \bar{m} + \bar{m}L)\, NN_{\mathrm{LLR}} + (2\bar{m} + N_A - 2)\, L + m(m-1)N/2$.

Table 3 summarizes the storage complexity of the optimized A-MLBIPCM, A-BIPCM, and MLPCM at 64-QAM and 256-QAM, where $N_{\mathrm{LLR}} = 8$. From Table 3, the storage complexity of A-MLBIPCM is higher than that of MLPCM but lower than that of A-BIPCM. Also, symbol likelihoods take up large proportion of storage, which means a lower V can help to reduce the storage complexity of A-MLBIPCM. Through optimization on encoding pattern and V, A-MLBIPCM can provide 23.84%–27.34% savings in storage complexity compared with A-BIPCM.

6 Conclusion

A low-complexity polar-coded modulation is proposed, which utilizes spatial coupling and multilevel structures, referred to as A-MLBIPCM. Simulation results show that A-MLBIPCM with optimal encoding and modulation patterns provides better BLER performance than MLPCM due to its spatial coupled structure. Compared with A-BIPCM, A-MLBIPCM takes advantage of multilevel structure, which leads to 23.84%–27.34% lower storage complexity and up to 33.02% lower decoding complexity with comparable BLER performance.

Acknowledgements This work was supported by National Key Research and Development Project (Grant No. 2020YFB1806805).

References

1 Arikan E. Channel polarization: a method for constructing capacity-achieving codes for symmetric binary-input memoryless channels. IEEE Trans Inform Theor, 2009, 55: 3051–3073
2 Seidl M, Schenk A, Stierstorfer C, et al. Polar-coded modulation. IEEE Trans Commun, 2013, 61: 4108–4119
3 Dai J, Piao J, Niu K. Progressive rate-filling: a framework for agile construction of multilevel polar-coded modulation. IEEE Wireless Commun Lett, 2021, 10: 1123–1127
4 Chen P, Bai B. Design and performance of the polar coded modulation for high mobility communications. In: Proceedings of IEEE 87th Vehicular Technology Conference (VTC Spring), Porto, 2018. 2577–2465
5 Liu L, Yan Y, Ling C, et al. Construction of capacity-achieving lattice codes: polar lattices. IEEE Trans Commun, 2019, 67: 915–928
6 Chandesris L, Savin V, Declercq D. Lasting successive cancellation based decoders for multilevel polar coded modulation. In: Proceedings of the 25th International Conference on Telecommunications (ICT), St. Malo, 2018. 264–268
7 Dai J, Niu K, Si Z, et al. Polar-coded spatial modulation. IEEE Trans Signal Process, 2021, 69: 2203–2217
8 Chen K, Niu K, Lin J R. An efficient design of bit-interleaved polar coded modulation. In: Proceedings of 2013 IEEE 24th Annual International Symposium on Personal, Indoor, and Mobile Radio Communications (PIMRC), London, 2013. 693–697
9 Bioglio V, Gabry F, Land I, et al. Multi-kernel polar codes: concept and design principles. IEEE Trans Commun, 2020, 68: 5350–5362
10 Mahdavifar H, El-Khamy M, Lee J, et al. Polar coding for bit-interleaved coded modulation. IEEE Trans Veh Technol, 2015, 65: 3115–3127
11 Wu X, Qiu M, Yuan J. Partially information coupled bit-interleaved polar coded modulation. IEEE Trans Commun, 2021, 69: 6409–6423
12 Iscan O, Bohnke R, Xu W. Shaped polar codes for higher order modulation. IEEE Commun Lett, 2018, 22: 252–255
13 Iqbal S, Kaminski P M, Klejs F, et al. Probabilistically shaped rate-adaptive polar-coded 256-QAM WDM optical transmission system. J Lightwave Technol, 2020, 38: 1800–1808
14 Fayyaz U U. Symbol mapping design for bit-interleaved polar-coded modulation with iterative decoding. IEEE Commun Lett, 2019, 23: 32–35
15 Dai J, Niu K, Si Z. Asynchronous polar-coded modulation. In: Proceedings of IEEE International Symposium on Information Theory (ISIT), Los Angeles, 2020. 1–6
16 Isaka M, Imai H. Hierarchical coding based on adaptive multilevel bit-interleaved channels. In: Proceedings of IEEE 51st Vehicular Technology Conference, Tokyo, 2000. 2227–2231
17 Xiao B, Xiao K, Chen Z, et al. Joint design for modulation and constellation labels in multiuser superposition transmission. IEEE Trans Broadcast, 2019, 65: 245–259
18 Zhang L, Wu Y, Li W, et al. Layered-division multiplexing: an enabling technology for multicast/broadcast service delivery in 5G. IEEE Commun Mag, 2018, 56: 82–90
19 Li Q, Zhang J, Bai L, et al. Performance analysis and system design for hierarchical modulated BICM-ID. IEEE Trans Wireless Commun, 2014, 13: 3056–3069
20 Park S I, Lee J Y, Myoung S, et al. Low complexity layered division multiplexing for ATSC 3.0. IEEE Trans Broadcast, 2016, 62: 233–243
21 Lampe L H J, Schober R, Fischer R F H. Multilevel coding for multiple-antenna transmission. IEEE Trans Wireless Commun, 2004, 3: 203–208
22 Balogun P R, Marsland I D, Gohary R H, et al. Polar code design for irregular multidimensional constellations. IEEE Access, 2017, 5: 21941–21953